Yuliang Xie
Department of Chemical Engineering,
The Pennsylvania State University,
University Park,
State College, PA 16802

Zhangming Mao
Department of Engineering Science and Mechanics,
The Pennsylvania State University,
University Park,
State College, PA 16802

Hunter Bachman
Department of Mechanical Engineering and Materials Science,
Duke University,
Durham, NC 27708

Peng Li
Department of Engineering Science and Mechanics,
The Pennsylvania State University,
University Park,
State College, PA 16802

Peiran Zhang
Department of Mechanical Engineering and Materials Science,
Duke University,
Durham, NC 27708

Liqiang Ren
Department of Engineering Science and Mechanics,
The Pennsylvania State University,
University Park,
State College, PA 16802

Mengxi Wu
Department of Mechanical Engineering and Materials Science,
Duke University,
Durham, NC 27708

Tony Jun Huang[1]
Department of Mechanical Engineering and Materials Science,
Duke University,
Durham, NC 27708
e-mail: tony.huang@duke.edu

Acoustic Cell Separation Based on Density and Mechanical Properties

Density and mechanical properties (e.g., compressibility or bulk modulus) are important cellular biophysical markers. As such, developing a method to separate cells directly based on these properties can benefit various applications including biological research, diagnosis, prognosis, and therapeutics. As a potential solution, surface acoustic wave (SAW)-based cell separation has demonstrated advantages in terms of biocompatibility and compact device size. However, most SAW-reliant cell separations are achieved using an entangled effect of density, various mechanical properties, and size. In this work, we demonstrate SAW-based separation of cells/particles based on their density and compressibility, irrespective of their sizes, by manipulating the acoustic properties of the fluidic medium. Using our platform, SAW-based separation is achieved by varying the dimensions of the microfluidic channels, the wavelengths of acoustic signals, and the properties of the fluid media. Our method was applied to separate paraformaldehyde-treated and fresh Hela cells based on differences in mechanical properties; a recovery rate of 85% for fixed cells was achieved. It was also applied to separate red blood cells (RBCs) and white blood cells (WBCs) which have different densities. A recovery rate of 80.5% for WBCs was achieved. [DOI: 10.1115/1.4046180]

Keywords: surface acoustic wave (SAW), cell separation, cell density, cell mechanical properties

Introduction

Cell density and mechanical properties (e.g., bulk modulus or compressibility) are important for cellular phenotyping, diagnosis, and prognosis [1–4]. For example, changes in the densities of red blood cells (RBCs) can be an indicator of membrane loss, abnormal surface-to-volume ratios, and/or alterations to the intracellular ion count or water content [5]. Additionally, RBCs have a greater density than white blood cells (WBCs) due to the presence of highly concentrated hemoglobin; this density difference provides a criterion for cell separation. The abnormal mechanical properties of cells can often be linked to inherited genetic disorders (e.g., sickle cell anemia and hereditary spherocytosis), noninfectious diseases (e.g., diabetes and cancer), or infectious diseases (e.g., malaria) [6–8]. Given these facts, methods that can rapidly separate cells of different densities, as well as mechanical properties, are critical for detecting diseases such as cancers and infections, and they also benefit many applications in biology, chemistry, and medicine [9–14].

Density-based cell separation is conventionally achieved with centrifugation [15]. Despite its robust performance, the process of centrifugation exerts strong rotational forces on cells which might

[1]Corresponding author.

Manuscript received November 5, 2019; final manuscript received December 30, 2019; published online February 28, 2020. Assoc. Editor: Victor H. Barocas.

alter their natural functionality, and requires bulky instrumentation. On the other hand, separating cells based on differences in mechanical properties usually relies on interactions between cells and cell-sized structures (e.g., pores, pillars, curves, and narrow channels) in either bulk or microfluidic devices [16–22]. For example, Yang et al. [23] demonstrated fresh/fixed RBC separation by manipulating the trajectories of either subgroup after passing through a narrow channel while suspended in a viscoelastic media; Holmes et al. [24] showed that RBCs treated with different concentrations of glutaraldehyde display a varied displacement in a deterministic lateral displacement device. Hvichia et al. utilized cell-sized microfluidic channel to separate circulating tumor cells from WBCs 25], which features larger deformability (i.e., softer) than WBCs. Nevertheless, using devices with numerous cell-sized structures that contact cells increases the risk of clogging or contact-based damage to the cells. Therefore, it is desirable to develop a cell density and mechanical property-based separation method that is compact, noncontact, and does not disrupt cellular functions.

The surface acoustic wave (SAW) [26–28] has demonstrated great momentum in cell separation [29–37] due to its compact, noncontact, and biocompatible operation [38–42]. Traditionally, to separate cells in an acoustofluidic (i.e., the fusion of acoustics and microfluidics) device, a SAW field is established in a two-dimensional (2D) plane that is parallel [43] or tilted [44] with respect to a microfluidic channel [45,46]; cells passing through this SAW field deflect in response to acoustic radiation forces [47,48]. The most widely used SAW separation mechanisms are based on an integrated effect of cell size, density, and mechanical properties [49] in which the cell size is often the dominant factor. As an example, since the range of densities present in a cell population may be very narrow [2], the cellular mass and volume, which may vary by as much as 50%, have a much greater impact on distinguishing different cell types during acoustic radiation force-based separation. However, utilizing a method that is heavily dependent on size may mask differences in compressibility or other mechanical properties that are present between different cell types. In another case, metastatic cancer cells show a similar volume but "softer" phenotype to that of their healthy counterparts due to the changes in the cytoskeleton structures [9,50]; in both cases, a cell's density and mechanical properties, rather than size, may provide more appropriate parameters to distinguish between cell populations.

In this work, we present an effort to decouple the effects of size from density and other mechanical properties during acoustic cell separation by adjusting the acoustic properties (i.e., density and/or speed of sound) of the fluidic medium. Manipulating the fluid properties allows us to determine whether cells equilibrate at positions of pressure nodes (PNs) or antinodes (ANs). In addition, since all the cells migrate to their equilibrium positions at either pressure nodes or antinodes, regardless of their initial positions, this separation approach no longer requires a sheath flow to set the initial positions of cells. To demonstrate the design, mechanism, and performance of our cell separation platform, we first conducted a numerical simulation to elucidate the mechanism of particle/cell migration due to the acoustic radiation force. Second, we demonstrated the capability of our acoustofluidic devices in separating polydimethylsiloxane (PDMS) and polystyrene microparticles in water. Third, we added Ficoll to the fluidic domain to modify its properties and separate different cell types. We demonstrated density-based (i.e., RBCs and WBCs) and compressibility (or bulk modulus)-based (i.e., paraformaldehyde-treated and fresh *Hela* cells) cell separations. With the ability to separate cells with different densities and mechanical properties, the application of our contactless, biocompatible SAW separation technology is expected to be a powerful tool in many biological, chemical, biophysical, and medical applications.

Methods

Materials. Ficoll (MW = 70 and 400 kDa) were purchased from Millipore-Sigma (Burlington, MA). Polystyrene microparticles with fluorescence (excitation at 480 nm; emission at 520 nm) (Warrington, PA) and 5 μm diameter were purchased from Polysciences, Inc. PDMS microparticles were prepared following the protocol. A single gram of a 10:1 mixture of PDMS prepolymer to curing agent (Sylgard 184, Dow Corning, Inc., Freeland, MI) was combined with a 1% (w/w) sodium dodecyl sulfate solution; we sonicated this solution for 20 min to emulsify the PDMS polymer with the sodium dodecyl sulfate, and then incubated the mixture at 65 °C for 60 min and left it at ambient conditions for 12 h to allow curing.

Cells. *Hela* cells were grown in Dulbecco's Modified Eagle Medium: Nutrient Mixture F-12 (DMEM/F12) media (Fisher Scientific, Hampton, NH), supplemented with 10% fetal bovine serum (R&D Systems, Minneapolis, MN), penicillin (100 U/mL), and 100 μg/mL streptomycin (Mediatech, Manassas, VA). The cell lines were maintained in T-25 cell culture flasks in a 37 °C incubator at 5% CO_2 and were cultured twice per week. Before each experiment, an adherent culture was released from flasks using 0.05% trypsin digestion (Cellgro, Corning, NY), and was rinsed with Trypsin neutralizer solution (Life Technologies, Carlsbad, CA). After centrifugation at 800 rpm for 5 min and rinsing with phosphate-buffered saline (PBS) buffer (1×, *p*H 7.4), cells were resuspended in a PBS solution for experiments. To change the mechanical properties of *Hela* cells, they were treated using 4% (wt/vol) paraformaldehyde (Santa Cruz Biotechnology, Dallas, TX) for 10 min at room temperature, then were resuspended in a PBS solution.

Blood cells collected within 24 h of experiments were first lysed using RBC lysis buffer for 5 min to remove most erythrocytes. WBCs were collected by centrifuging the blood at 800× *g* and resuspended in the same volume as the whole blood in 1× PBS solution with 0.1% pluronic F-68. To prepare samples with predefined ratio between RBCs and WBCs, the suspended WBC sample was mixed with a certain volume of whole blood.

Microfluidic Setup. Chrome-plated gold (Cr/Au, 50 Å/500 Å) was deposited onto a 128 deg Y-cut lithium niobate ($LiNbO_3$) wafer (500 μm thick) that had been patterned with a photoresist, followed by a liftoff technique to form the pair of interdigital transducers (IDTs). The PDMS-based microchannel was fabricated per a standard soft-lithography and replica molding procedure using SU-8 photoresist. Holes were punched in the PDMS microchannel for inlets and outlets with a Harris Uni-Core 1.0 mm punch. To bond the PDMS microchannel with a $LiNbO_3$-based SAW substrate, a plasma cleaner (Harrick Plasma, Ithaca, NY) was used to treat the components with oxygen plasma for 3 min. The PDMS microchannel was aligned and bonded to the SAW substrate between the IDTs. The whole device was cured for at least 3 days in a 65 °C oven before being used in testing; this was done to avoid leakage between the channel and the SAW substrate.

We completed our testing using an inverted microscope (Nikon Eclipse Ti-U, Japan). To eliminate the virtual image from the double-side polished $LiNbO_3$ substrate, a polarizer was placed in the light path and adjusted to the requisite angle. Sample solutions were prepared in 1 ml plastic syringes (Becton, Dickinson and Company, Franklin Lakes, NJ), such that a syringe pump (neMESYS, cetoni GmbH, Germany) could be used to deliver the fluid into the channel through polyethylene tubing (Becton, Dickinson and Company). To control the flow, one pump injected samples from the inlet; two other pumps were connected to the outlets for withdrawal; and the last outlet was open. Radiofrequency signals were generated (E4422B, Agilent, Santa Clara, CA) at desired frequencies and were amplified (100A250A, Amplifier Research, Souderton, PA) to generate the standing SAW fields. A CCD camera (Coolsnap HQ2, Photometrics, Tucson, AZ) was positioned facing the *XY* plane of the device to record the motion of microparticles at 10 fps. The trajectories of particles during

particle separation were generated using IMAGEJ software to stack the recorded video.

Recovery Rate. The recovery rate of a specific type of particles/cells collected from an outlet was calculated from the following equation:

$$\text{recovery rate} = \frac{c_1 v_1}{c_0 v_0} \tag{1}$$

where c_1 is the concentration of a specific particle, v_1 is the flowrate from a specific outlet, c_0 is the original concentration of particles at the inlet, and v_0 is the flowrate from the inlet. The recovery rate was calculated with three experimental replications and represented by mean ± standard deviation.

Viability Test. The viability of WBCs and *Hela* cells is tested to verify biocompatibility of the separation process. Tested cells were immersed at the highest concentration of Ficoll which we have used in separation experiments (30% w/w), and then flowed through the microfluidic channel with a flowrate of 10 μL/min and an acoustic power of −8 dBm (maximum power used in experiments). Cells were collected from the outlet during a 15 min operation period. The WBCs were stained with propidium iodide. As control groups, viability tests were conducted on cells that were immersed in Ficoll without SAW, PBS without SAW, and ethanol. In addition, *Hela* cells were collected at the outlets, they were transferred to a DMEM/F12 medium and cultured at 37 °C for growth testing.

Numerical Methods. The SAW-induced acoustic field distribution and the particle motion were numerically studied using COMSOL MULTIPHYSICS 4.4. The SAW field was simulated with the pressure acoustics module using a frequency domain study. Particle trajectories were simulated with the particle tracing for fluidic flow module. To simplify the model, the standing SAWs were considered uniform along the longitudinal direction of the channel; the acoustic field and the resulted particle migration in a 2D channel cross section were numerically investigated to simplify the analysis of three-dimensional motion of the particles. In addition, the piezoelectric substrate and the PDMS channel were not included in the 2D numerical model, and their physical effects on the acoustic field in the fluid were modeled by boundary conditions. These simulations also solved the acoustic radiation force, the Stokes drag force, and the particles' motion in the lateral direction (x–z plane). Parameters used in this numerical study were listed in Tables 1 and 2.

The governing equation for the acoustic field p in the fluid domain was the lossy Helmholtz equation, given as [51]

$$\frac{\omega^2}{c_f^2} p + \left[1 + \frac{i\omega(1+\beta)\mu}{\rho_f c_f^2}\right] \nabla^2 p = 0 \tag{2}$$

Table 1 Parameters of liquids and particles used in numerical simulations

	Water	Polystyrene	PDMS
Density (kg/m^3)	997	1050	965
Speed of sound (m/s)	1495	2350	1080
Dynamic viscosity (Pa·s)	0.001	N/A	N/A

Table 2 Parameters of SAWs used in simulations

Acoustic phase velocity of SAW (m/s)	3900
Frequency (MHz)	13
Amplitude of vibration of SAW (nm)	1

where p, ρ_f, c_f, ω, β, μ, and i indicate, respectively, the acoustic pressure, density of fluid, acoustic phase velocity of fluid, angular velocity, fluid viscosity ratio, fluid dynamic viscosity, and imaginary unit. The acoustic particle velocity $\boldsymbol{v}$ (acoustic particle velocity) was coupled with the acoustic pressure p via the momentum balance equation in fluid

$$\boldsymbol{v} = -\frac{\nabla p}{i\omega\rho_f}\left[1 + \frac{i\omega(1+\beta)\mu}{\rho_f c_f^2}\right] \tag{3}$$

This equation gave the velocity field $\boldsymbol{v}$ corresponding to a given pressure from Eq. (2), which was solved by establishing boundary conditions. The bottom of the 2D fluid domain was the actuation boundary of the standing SAW, which was modeled as the acceleration of surface particles moving transversely

$$\boldsymbol{a} = -\boldsymbol{n}\left[\frac{\nabla p}{\rho_f}\left[1 + \frac{i\omega(1+\beta)\mu}{\rho_f c_f^2}\right]\right] = \boldsymbol{n} \cdot A_0\omega^2\left[e^{-ik_s x} - e^{-ik_s(w_0 - x)}\right] \tag{4}$$

where A_0, k_s, w_0, and $\boldsymbol{n}$ correspond to the amplitude of SAW displacement, wave number of SAW, channel width, and boundary normal vector, respectively. The other three boundaries are defined as lossy [51] to model the acoustic pressure loss upon propagation through the PDMS/fluid interface

$$\boldsymbol{n} \cdot \nabla p = i\frac{\omega\rho_f}{\rho_w c_w} p \tag{5}$$

where ρ_w and c_w are the density and the speed of sound in the wall's material, respectively.

Once the acoustic fields p and $\boldsymbol{v}$ are obtained from the 2D model, the time-averaged acoustic potential in the fluid domain and acoustic radiation force on a single spherical particle can be calculated by the following equations [52]:

$$\boldsymbol{U} = V_0\left[f_1 \frac{1}{4\rho_f c_f^2}\text{Re}(p \cdot p^*) - f_2 \frac{3\rho_f}{8}\text{Re}(v \cdot v^*)\right] \tag{6}$$

$$\boldsymbol{F}_{\text{rad}} = -\nabla U \tag{7}$$

In Eq. (6), V_0 is the particle volume; ρ_p and c_p are the density and sound speed of the particle, respectively; Re is the real part of a complex value; and the asterisk indicates complex conjugation. Two parameters in Eq. (7), i.e., $f_1 = 1 - (\rho_f c_f^2)/(\rho_p c_p^2)$, and $f_2 = 2(\rho_p - \rho_f)/(2\rho_p + \rho_f)$, determine the direction of the particles' motion, based on their densities and speed of sound, which is closely related with the compressibility and bulk modulus.

Results and Discussion

Working Mechanism. The acoustofluidic cell separation device included a microfluidic channel for sample handling and a pair of IDTs for acoustic actuation (Fig. 1(*a*)). The single-layer microfluidic channel had a single inlet and three outlets. The dimensions of microfluidic channel within the particle/cell deflection region were 340 μm in width, 60 μm in depth, and 10 mm in length. The IDT pairs were positioned parallel to the microfluidic channel. Each IDT contained 20 pairs of electrodes each 10 mm in length and a gap between each electrode 150 μm, yielding in an operating frequency of 12.89 MHz (Fig. 1(*b*)). This operational frequency enabled us to establish three low pressure zones and two high pressure zones in the channel, as described in the following discussion.

The design of the separation system was guided by numerical studies into the acoustic pressure distributions and particle

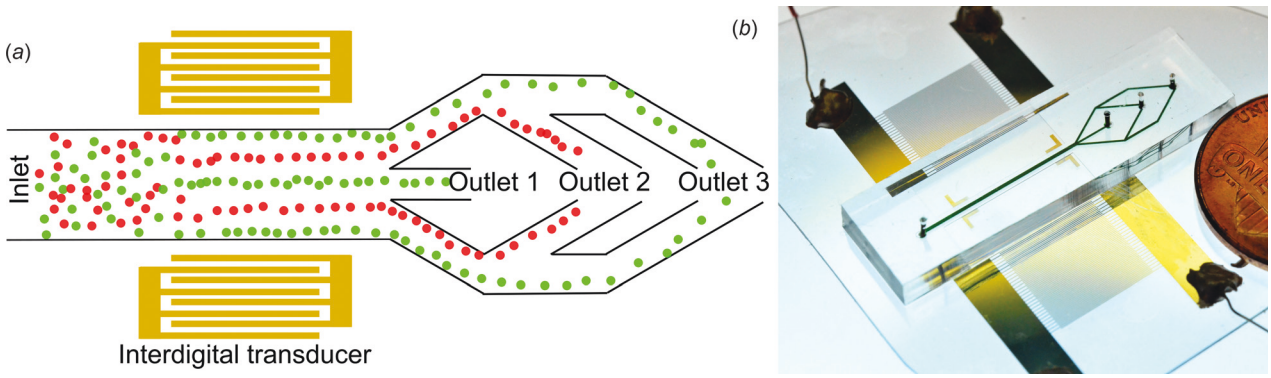

Fig. 1 (*a*) Schematic and (*b*) photo of the acoustic cell separation device

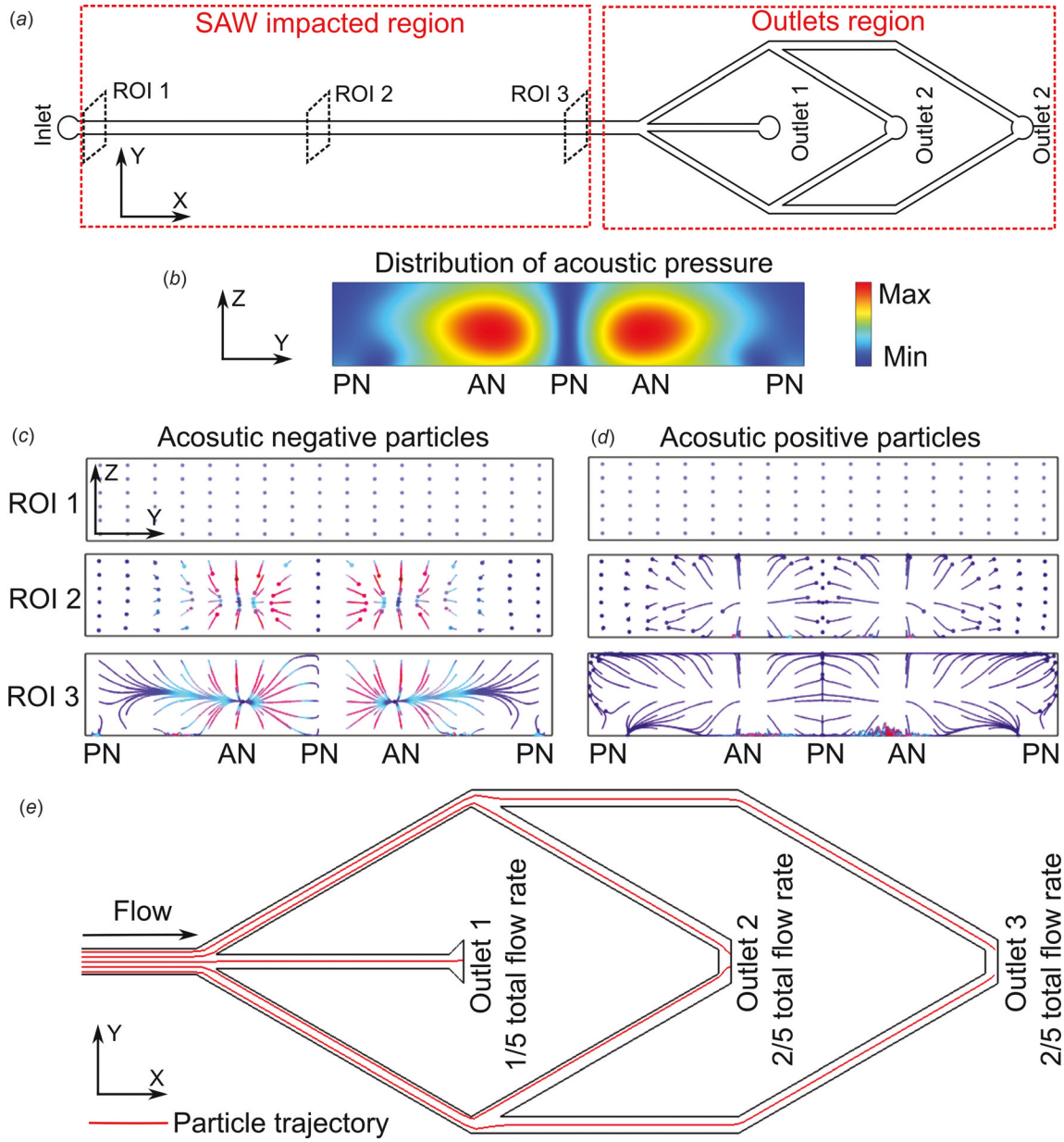

Fig. 2 (*a*) Numerical studies conducted in the SAW-impacted region and outlet region. (*b*) The distribution of acoustic pressure distributions in the SAW-impacted region, where a position with minimum acoustic pressure is named a PN and a position with maximum pressure is named a pressure AN. ((*c*) and (*d*)) The simulated trajectories of acoustic negative and positive particles in the standing SAW field. (*e*) Simulated trajectories of particles in the outlet region, where particles start at equilibrium positions at the end of SAW impact region, and follow laminar flow to each collecting outlets.

motions in the SAW region and outlet region of the device (Fig. 2(*a*)). In the SAW-impacted region, two parallel IDTs generated a two-dimensional standing acoustic field in the channel that was symmetric in the *Y*-direction. Aligning the microfluidic channel and the IDTs produced two maximum acoustic pressure lines (i.e., pressure antinode lines) and three minimum pressure lines (i.e., pressure node lines). The pressure nodes were located at the two edges and the center of the channel, and the antinodes were located in between (Fig. 2(*b*)). Using our simulations, we showed that when randomly distributed particles of lesser density and/or bulk modulus (i.e., slower speed of sound, and larger compressibility) than those of the fluid medium are exposed to the acoustic field shown in Fig. 2(*b*), they will move to the pressure antinodes (Fig. 2(*c*)) according to Eq. (6). To simplify our description of this phenomenon, particles migrating to pressure antinodes were referred to as "acoustic negative particles." Conversely, particles with larger density and speed of sound than surrounding medium, referred to as "acoustic positive particles," move to the pressure nodes (Fig. 2(*d*)). We also simulated the motion of acoustic positive/negative particles along the length of the channel, and demonstrated that the PDMS and polystyrene particles align on opposite nodes (Fig. S1 available in the Supplemental Materials on the ASME Digital Collection.). After particles exit the SAW-impacted region of the device, a branched channel was designed to collect particles at specific outlets. This design was guided by the motion of particles in the laminar flow field. The red lines shown in the simulation of Fig. 2(*e*) provide the trajectories of particles which originated at the equilibrium positions of particles in the standing SAW field. These simulation results showed that the two particle trajectories which originated from the pressure antinodes would flow toward outlet 2, whereas the lines originating from the pressure nodes would flow to outlets 1 and 3 (Fig. 2(*e*)).

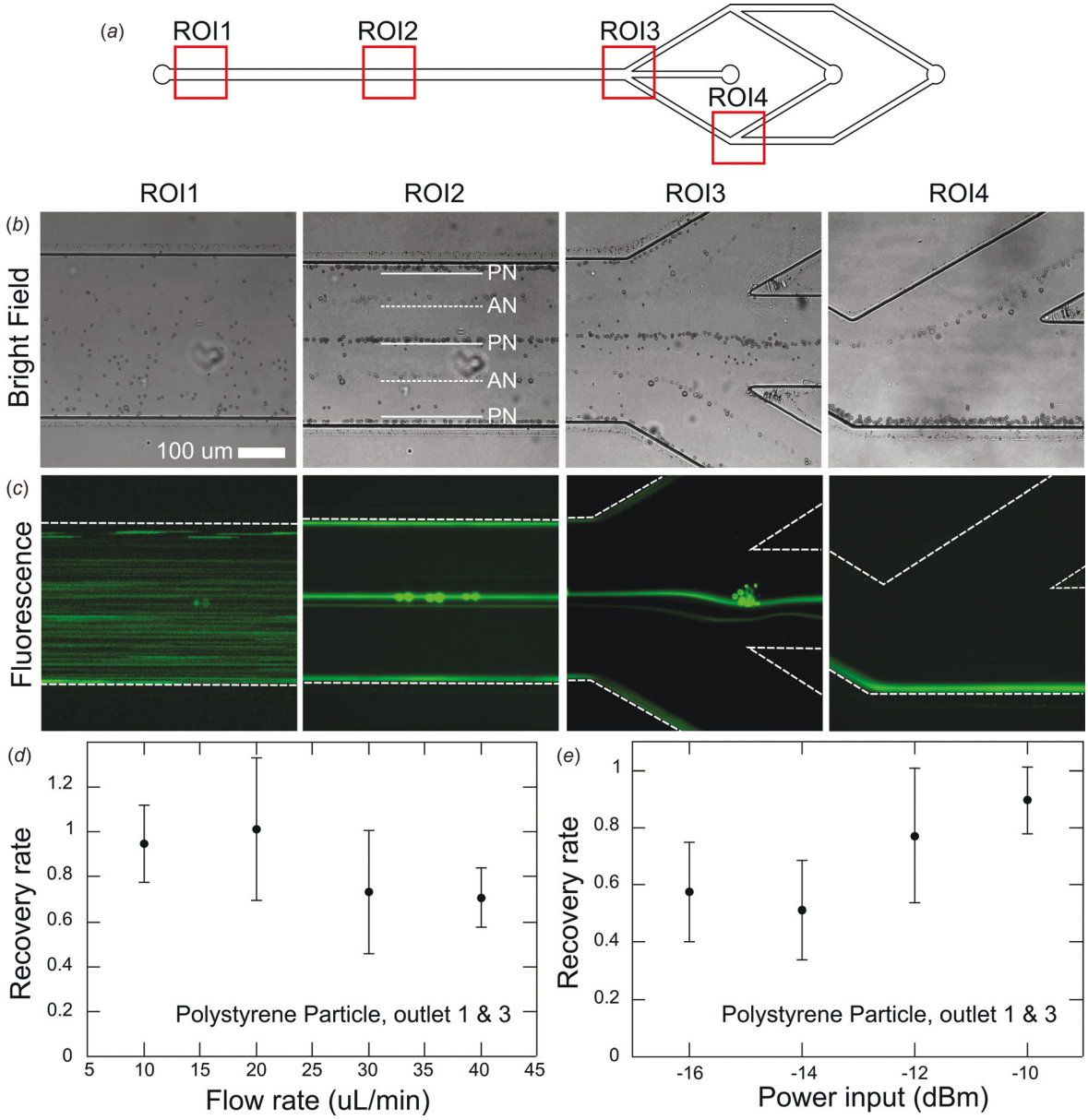

Fig. 3 (*a*) **Separation of PDMS and polystyrene particles in water.** (*b*) **Bright-field images of the trajectories of PDMS and polystyrene particles, where polystyrene particles focused at three PNs and PDMS particles focused at two pressure ANs.** (*c*) **Fluorescent images of the trajectories of polystyrene particles that focused at three PNs. The recovery rates of polystyrene particles collected from outlets 1 and 3 at** (*d*) **different flowrates and a constant −10 dBm power input, and** (*e*) **different power inputs and a constant flowrate of 20 μL/min.**

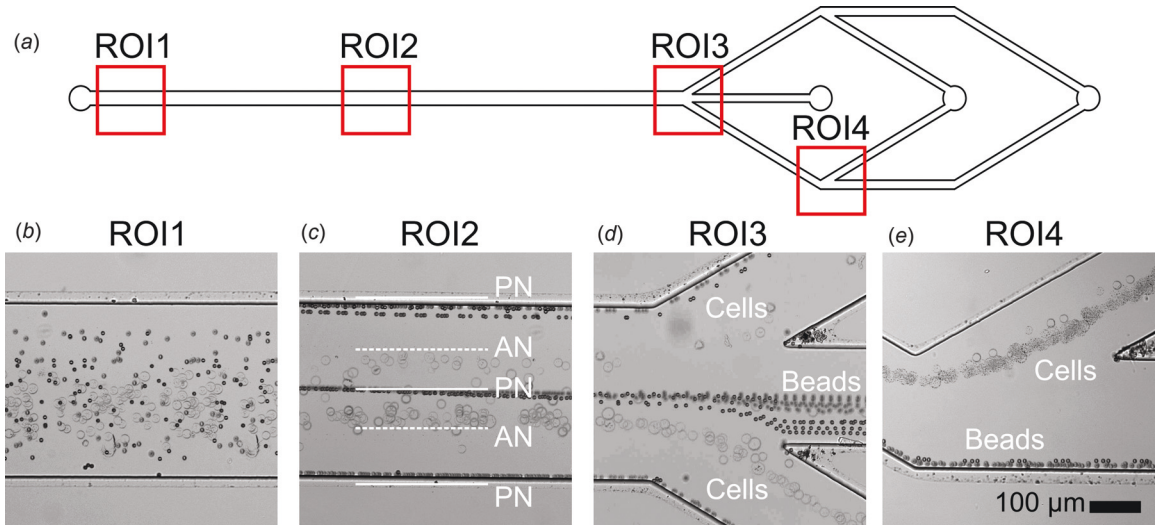

Fig. 4 (*a*) Motion of *Hela* cells and polystyrene particles in 25% (w/w) Ficoll medium at different ROIs. (*b*) A mixture of *Hela* cells and polystyrene beads before SAW-impacted region, ROI 1. (*c*) *Hela* cells move to pressure antinodes, while polystyrene particles move to pressure nodes in the SAW-impacted region, ROI 2. ((*d*) and (*e*)) At the outlet regions ROI 3 and ROI 4, *Hela* cells and polystyrene particles were collected from the corresponding outlets.

Separation of Polystyrene and Polydimethylsiloxane Particles. Once we verified the mechanism of our acoustic separation device through simulations, we experimentally tested our device's ability to separate PDMS (polydisperse diameters, 1–20 μm) and polystyrene particles (diameter 5 μm) in water (Fig. 3). In this demonstration, the PDMS particles have a lower density and higher compressibility than water, meaning that they should move to the pressure antinodes; the relatively stiff polystyrene particles should aggregate at the pressure nodes. From region of interest (ROI) 1 of Figs. 3(*b*) and 3(*c*), it can be seen that the mixture of particles was distributed randomly before the SAW-impacted region. When particles flowed through the SAW-impacted region, they were focused into five lines (ROI 2, Fig. 3(*b*)). Fluorescent images confirmed that polystyrene particles with green fluorescence focused at the three pressure node lines at the sidewalls and the center of the channel, and the bright field images confirmed that the PDMS particles aligned along the antinode lines (ROI 2, Fig. 3(*c*)). The focused particles exited from the SAW-impacted regions to the outlets. The polystyrene particles that were focused at the central line flow out at outlet 1 (ROI 3, Fig. 3(*b*)); polystyrene particles focused at the two edges of the channel were collected at outlet 3 (ROI 4, Fig. 3(*c*)). The two lines of focused PDMS particles were collected at outlet 2 (ROI 4, Fig. 3(*b*)).

The recovery rate of polystyrene particles collected from outlets 1 and 3 was calculated according to Eq. (1) at different flowrates and power inputs. To test the effect of the flowrate, the recovery rate of polystyrene particles from outlets 1 and 3 was evaluated at flowrates from 10, 20, 30, and 40 μL/min, and a constant −10 dBm of power input (Fig. 3(*d*)). At flowrates of 10 and 20 μL/min, the average recovery rate of the polystyrene particles was 95% and 99%, respectively, indicating that almost all of the particles were collected from the expected outlets. When the flowrate increased to 30 μL/min, the recovery rate began to decrease, falling to 73%; at the largest flowrate tested in the experiments (40 μL/min), the particle recovery rate dropped to 70%. When the flowrate increased, the time that the particles spent in the SAW region was reduced, interrupting the particles' migration to their equilibrium positions and resulting in a lower recovery rate. We also explored how the power input influences the recovery rate of polystyrene particles (Fig. 3(*e*)). We found that at a constant flowrate of 20 μL/min and lower power inputs (−16 and −14 dBm), the recovery rate was also low because the weak acoustic radiation force was not sufficient to move particles to their equilibrium positions. This was resolved when the power input was increased to −12 and −10 dBm, where the particle recovery rate increased to 90%.

The numerical and experimental exploration of PDMS and polystyrene particle separation demonstrated several key features of our technique. First, this separation mechanism is based on the difference in physical properties, rather than the size, of particles. Despite wide distributed size of PDMS particles (i.e., 1 to 20 μm), they all focused at pressure antinodes that were distinct from the polystyrene particles' equilibrium positions. However, although the separation mechanism is independent of the size of the particles, the authors would like to note that size still plays a factor in the efficiency of this separation, and the device may not be able to separate particles of any size. That is, particles that are too small (diameter less than 1 μm) are difficult to focus since the acoustic radiation force is proportional to the volume of particles. Nonetheless, with sufficient power and active IDT length, smaller particles could eventually reach their equilibrium positions with this technique. Second, this method does not require a sheath flow to establish the initial positions of particles/cells; this means that only a single inlet is needed to inject the mixture of particles, simplifying the control of the system. Third, the throughput of separation could potentially be improved by increasing the channel width and the flowrate. We designed a cell separation channel with double the width (640 μm); in this design, the particles were focused into nine lines (five lines for polystyrene particles and four lines for PDMS particles), while other operation properties were unchanged (Fig. S2 available in the Supplemental Materials on the ASME Digital Collection.). The increased number of node/antinode lines in this device allows us to increase the total flowrate while maintaining the channel flow velocity and device performance.

Particle/Cell Separation by Adjusting Acoustic Properties of the Fluidic Medium. PDMS and polystyrene particles can be separated in water due to their inherent differences in density and compressibility. However, almost all cells (e.g., *Hela* cell and WBCs) have larger densities than water due to their cellular content; this means that they all tend to move to pressure nodes in

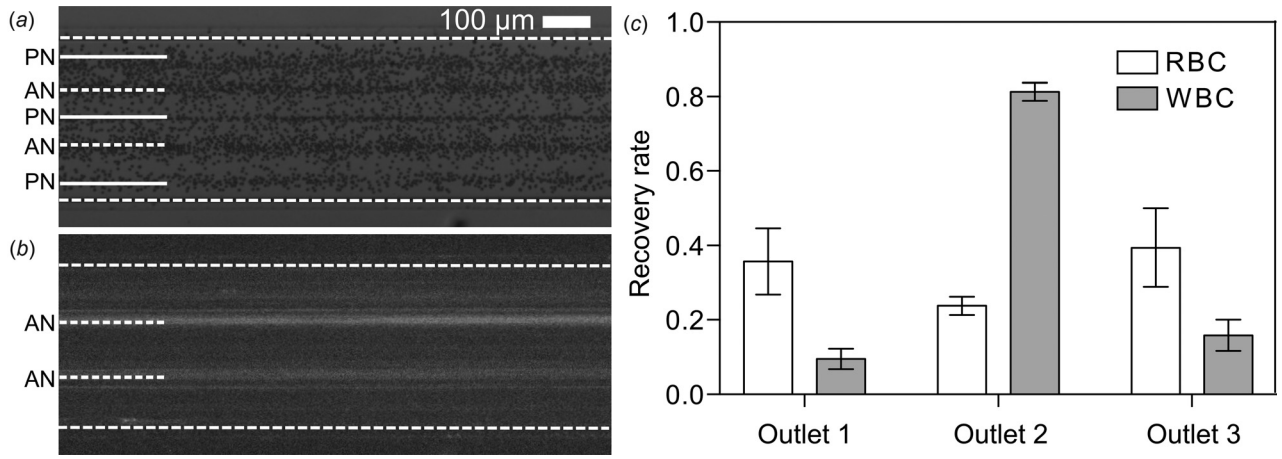

Fig. 5 Acoustic separation of RBCs and WBCs. (*a*) Bright-field images of WBC and RBC mixtures show the cells focused at five lines at positions of PNs and ANs. (*b*) Fluorescent image showing the trajectories of WBCs stained by Hoechst in the mixture, where WBCs are primarily focused at pressure ANs. (*c*) Plot of the recovery rate of RBCs and WBCs at three outlets.

water or buffer solutions, preventing acoustic separations using this mechanism. To separate different types of cells using our method, the acoustic properties of the fluidic medium need to be manipulated so that one cell type will become acoustically negative, while the other type of cell will remain acoustically positive. To achieve this manipulation, Ficoll was introduced into the suspension medium. Ficoll is a high-molecular weight sucrose-polymer formed by copolymerization of sucrose with epichlorohydrin [53–56]. The density of a Ficoll solution can be conveniently controlled by its concentration [57]. As such, by tuning the concentration of Ficoll, the equilibrium positions of cells can be manipulated to pressure nodes or antinodes. Additionally, research has shown that the addition of Ficoll to cell suspensions does not negatively affect the cell viability [57].

This exploitation was confirmed by analyzing the trajectories of *Hela* cells and polystyrene beads in 25% (w/w) Ficoll in PBS buffer (Fig. 4(*a*)). In PBS, both *Hela* cells and polystyrene particles would travel to pressure nodes. However, in the Ficoll solution, the *Hela* cells move to pressure antinodes (Fig. 4(*c*)) and are collected from outlet 2 (Fig. 4(*e*)). As expected, the polystyrene particles still migrated to the pressure nodes at the center and two edges of channel (Fig. 4(*c*)), and could be collected from outlets 1 and 3 (Fig. 4(*d*)). This phenomenon is consistent with the fact that although the density of polystyrene (1050 kg/m^3) is similar to that of *Hela* cells, the significantly greater speed of sound in polystyrene (2350 m/s) than water means that polystyrene particles remain acoustically positive. In addition, the *Hela* cells are still able to attach and culture after separation, indicating that the *Hela* cells remained intact in the Ficoll medium and under the influence of the SAWs.

Acoustic Cell Separation Based on Density. In this section, WBCs and RBCs were separated based on their differences in density. The separation of WBCs and RBCs has been proven as a very important process in many biomedical applications such as the proteomic or genomic analysis of WBCs [58], where blood samples need to be separated prior to analysis. However, using acoustic-based methods to separate RBCs from WBCs is challenging; although the volume of RBCs is less than WBCs, the larger densities of RBCs neutralize this difference so that the radiation forces on WBCs and RBCs are very similar. As such, modifying the fluid properties using our device should enable more efficient acoustic-based separation of RBCs and WBCs.

In the experiment, a spiked WBC and RBC sample was used to control their ratio between the cell types in the test sample. Specifically, WBCs collected from 1 mL of whole blood were suspended in a 30% (w/w) Ficoll solution in PBS; whole blood was added to the mixture to yield a final RBC/WBC ratio of

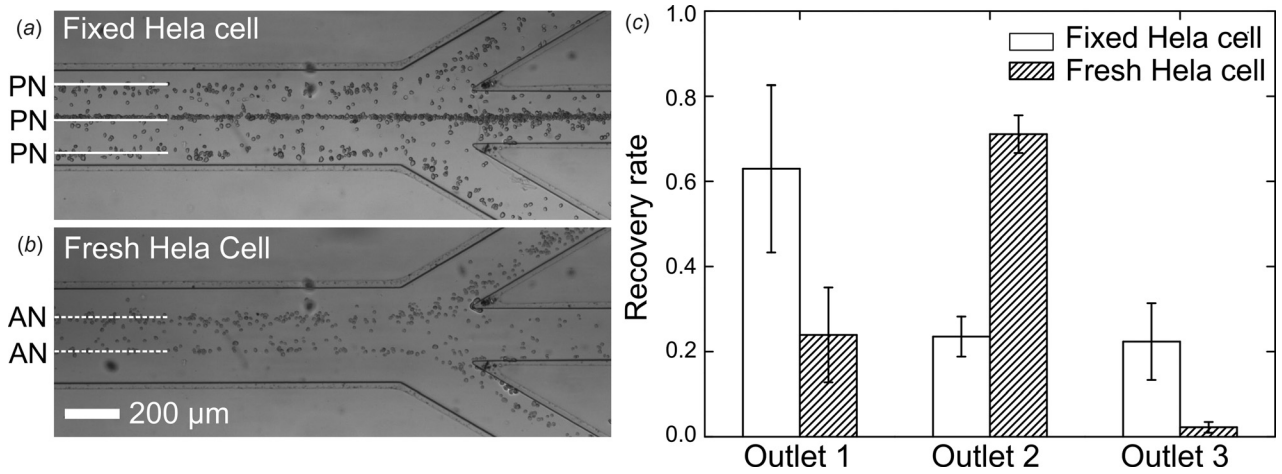

Fig. 6 Acoustic separation of fresh and paraformaldehyde treated *Hela* cells. (*a*) Paraformaldehyde-treated *Hela* cells focused into three lines at the positions of PNs. (*b*) Fresh *Hela* cells focused into two lines at the positions of the pressure ANs. (*c*) Plot of the recovery rate of the two different cell groups at the three outlets.

approximately 20:1. The mixture was injected into our acoustofluidic channel at a flowrate of 10 μL/min. After turning on the SAW, the blood cells in the channel focused into five lines (Fig. 5(*a*)). WBCs, visualized by staining of Hoechst, were mainly focused at the two pressure antinode lines (Fig. 5(*b*)). The separation performance was further studied quantitatively by counting the RBCs and WBCs collected at each outlet. We collected $\sim$100 μL cell suspensions from each outlet with the separation process running continuously for 30 min; the experiments were repeated three times and counting was done using a hemocytometer (Fig. S3 available in the Supplemental Materials on the ASME Digital Collection.). The recovery rate of WBCs at outlet 2 was 81.2$\pm$1.9% (mean $\pm$ standard deviation); for RBCs, the recovery rate at outlet 1 was 35.7$\pm$7.2%, and 39.4$\pm$8.6% at outlet 3, yielding a total recovery rate of 75.1$\pm$15.8% from the expected outputs (Fig. 5(*c*)). In addition, propidium iodide staining results showed that 87% WBCs were intact after Ficoll and SAW treatment (Fig. S4 available in the Supplemental Materials on the ASME Digital Collection.). The excellent biocompatibility of our method is not surprising because the chemical we added, Ficoll, has more than 50 years of history in processing WBCs and other cell lines with minimum cytotoxicity and osmotic pressures that keep cells intact [59]. Furthermore, we expected the SAW treatment to minimally perturb cells [60] as we have demonstrated in our previous work [61]. The combined use of these two methods should not impact the cell integrity.

Using our method, we were able to decouple the effect of cell size from cell density during acoustic separation. Controlling the fluid media allowed us to achieve the separation of RBCs and WBCs by selectively moving them toward pressure nodes/antinodes, respectively. However, the recovery rate of WBCs shown here was not perfect, which we largely suspect was due to heterogeneous properties of the cell populations. This is especially true for WBCs, as some cells present multiple nuclei, which vary the cell density and cause undesired cells motion [62]. Additionally, some of the RBCs that have densities close to the WBCs are inevitably collected from the incorrect outlet, which reduces the recovery rate of RBCs.

Acoustic Cell Separation Based on Mechanical Properties. To validate the potential for our device to separate cells based on their mechanical properties (e.g., bulk modulus or compressibility), a mixture of fresh and paraformaldehyde treated *Hela* cells was separated (Fig. 6). Obviously, these cell groups share similar sizes and total protein amounts; however, the paraformaldehyde treatment creates covalent chemical bonds between proteins in the cell [63]. Such bonds anchor soluble proteins to the cytoskeleton to increase the rigidity of the tissue [64]. Considering that the speed of sound associated with a given solid medium is determined by its mechanical properties, including its bulk modulus and shear modulus, the stiffening of the cytoskeleton due to paraformaldehyde treatment will affect the acoustic potential and radiation forces experienced by the cells. By choosing a proper medium, the acoustic radiation force will move the paraformaldehyde-treated cells (with larger bulk modulus, or less compressibility) to pressure nodes, while fresh cells will be moved to pressure antinodes, achieving cell separation.

In a 25% (w/w) Ficoll solution, paraformaldehyde-treated *Hela* cells focused into three lines (i.e., the middle of the channel and two lines near the channel wall) (Fig. 6(*a*)), matching with the positions of the pressure nodes. Conversely, fresh *Hela* cells focused into two lines, matching the positions of pressure antinodes in the channels (Fig. 6(*b*)). The recovery rate of the cell separation was also studied quantitatively using a hemocytometer to count the cell populations collected from each outlet (Fig. S5 available in the Supplemental Materials on the ASME Digital Collection.). For the flowrate of 5 μL/min, the recovery rate for fixed *Hela* cell was 62.9$\pm$19.6% for outlet 1 and 22.4$\pm$9.0% for outlet 3, yielding a total recover rate of 85.3$\pm$28.6% for the pressure node outlets; the recovery rate of fresh *Hela* cell at outlet 2 was 71.1$\pm$4.4% (Fig. 6(*c*)). The success of this experiment exemplified the capability of our method in size-independent cell separations and showed how the device could potentially be applied to separate cells that have biophysical markers for diseases such as cancers.

Conclusion

We demonstrated an acoustofluidic cell separation device that operates based on cell density and mechanical properties. By designing the acoustic wavelength, channel dimensions, and acoustic properties of fluid in the channel, particles/cells migrated toward the pressure node or antinode positions according to their density and mechanical properties to achieve separation. With this method, we separated RBCs from WBCs through the difference in their densities. We achieved an average recovery rate of 80.5% for WBCs. We also separated cells with different mechanical properties; as an example, *Hela* cells were treated with paraformaldehyde to increase their stiffness and mixed with fresh *Hela* cells for separation. The results showed an 85% recovery rate of fixed *Hela* cells from the designated outlets. Since this separation method features great biocompatibility, compact device design, and avoids sheath flows to simplify the operational procedure, it is expected to benefit many biological studies and clinical applications.

Acknowledgment

T. J. H. has four U.S. patents (Patent Nos.: 8,573,060; 9,608,547; 9,606,086; and 9,757,699) related to acoustofluidics and acoustic tweezers. He has also cofounded a start-up company, Ascent Bio-Nano Technologies, Inc., to commercialize technologies involving acoustofluidics and acoustic tweezers.

Funding Data

- National Institutes of Health (R01GM132603, UG3T R002978, R01 HD086325, R33CA223908, and R01GM127714; Funder ID: 10.13039/100000002).
- U.S. Army Medical Research Acquisition Activity (W81XWH-18-1-0242; Funder ID: 10.13039/100014055).
- National Science Foundation (ECCS-1807601; Funder ID: 10.13039/100000001).

References

[1] Di Carlo, D., 2012, "A Mechanical Biomarker of Cell State in Medicine," J. Lab. Autom., **17**(1), pp. 32–42.
[2] Grover, W. H., Bryan, A. K., Diez-Silva, M., Suresh, S., Higgins, J. M., and Manalis, S. R., 2011, "Measuring Single-Cell Density," Proc. Natl. Acad. Sci., **108**(27), pp. 10992–10996.
[3] Polacheck, W. J., Li, R., Uzel, S. G. M., and Kamm, R. D., 2013, "Microfluidic Platforms for Mechanobiology," Lab Chip, **13**(12), pp. 2252–2267.
[4] Liu, H., Tan, Q., Geddie, W. R., Jewett, M. A. S., Phillips, N., Ke, D., Simmons, C. A., and Sun, Y., 2014, "Biophysical Characterization of Bladder Cancer Cells With Different Metastatic Potential," Cell Biochem. Biophys., **68**(2), pp. 241–246.
[5] Huisjes, R., Bogdanova, A., van Solinge, W. W., Schiffelers, R. M., Kaestner, L., and van Wijk, R., 2018, "Squeezing for Life—Properties of Red Blood Cell Deformability," Front. Physiol., **9**, pp. 1–22.
[6] Hoffman, B. D., and Crocker, J. C., 2009, "Cell Mechanics: Dissecting the Physical Responses of Cells to Force," Annu. Rev. Biomed. Eng., **11**(1), pp. 259–288.
[7] Mao, X., and Huang, T. J., 2012, "Exploiting Mechanical Biomarkers in Microfluidics," Lab Chip, **12**(20), pp. 4006–4009.
[8] Suresh, S., 2007, "Biomechanics and Biophysics of Cancer Cells," Acta Biomater., **3**(4), pp. 413–438.
[9] Xu, W., Mezencev, R., Kim, B., Wang, L., McDonald, J., and Sulchek, T., 2012, "Cell Stiffness is a Biomarker of the Metastatic Potential of Ovarian Cancer Cells," PLoS One, **7**(10), p. e46609.
[10] Wei, F., Lillehoj, P. B., and Ho, C., 2010, "DNA Diagnostics: Nanotechnology-Enhanced Electrochemical Detection of Nucleic Acids," Pediatr. Res., **67**(5), pp. 458–468.

[11] Pisanic Ii, T. R., Zhang, Y., and Wang, T. H., 2014, "Quantum Dots in Diagnostics and Detection: Principles and Paradigms," Analyst, **139**(12), pp. 2968–2981.
[12] Ndukaife, J. C., Mishra, A., Guler, U., Nnanna, A. G. A., Wereley, S. T., and Boltasseva, A., 2014, "Photothermal Heating Enabled by Plasmonic Nanostructures for Electrokinetic Manipulation and Sorting of Particles," ACS Nano, **8**(9), pp. 9035–9043.
[13] Guo, F., French, J. B., Li, P., Zhao, H., Chan, C. Y., Fick, J. R., Benkovic, S. J., and Huang, T. J., 2013, "Probing Cell–Cell Communication With Microfluidic Devices," Lab Chip, **13**(16), pp. 3152–3162.
[14] Tsutsui, H., and Ho, C.-M., 2009, "Cell Separation by Non-Inertial Force Fields in Microfluidic Systems," Mech. Res. Commun., **36**(1), pp. 92–103.
[15] English, D., and Andersen, B. R., 1974, "Single-Step Separation of Red Blood Cells, Granulocytes and Mononuclear Leukocytes on Discontinuous Density Gradients of Ficoll-Hypaque," J. Immunol. Methods, **5**(3), pp. 249–252.
[16] Bow, H., Pivkin, I. V., Diez-Silva, M., Goldfless, S. J., Dao, M., Niles, J. C., Suresh, S., and Han, J., 2011, "A Microfabricated Deformability-Based Flow Cytometer With Application to Malaria," Lab Chip, **11**(6), pp. 1065–1073.
[17] Zhang, Z., Xu, J., Hong, B., and Chen, X., 2014, "The Effects of 3D Channel Geometry on CTC Passing Pressure-Towards Deformability-Based Cancer Cell Separation," Lab Chip, **14**(14), pp. 2576–2584.
[18] Wang, G., Mao, W., Byler, R., Patel, K., Henegar, C., Alexeev, A., and Sulchek, T., 2013, "Stiffness Dependent Separation of Cells in a Microfluidic Device," PLoS One, **8**(10), p. e75901.
[19] Van Den Bergh, J. P. W., Van Lenthe, G. H., Hermus, A. R. M. M., Corstens, F. H. M., Smals, A. G. H., and Huiskes, R., 2000, "Speed of Sound Reflects Young's Modulus as Assessed by Microstructural Finite Element Analysis," Bone, **26**(5), pp. 519–524.
[20] Wang, G., Crawford, K., Turbyfield, C., Lam, W., Alexeev, A., and Sulchek, T., 2015, "Microfluidic Cellular Enrichment and Separation Through Differences in Viscoelastic Deformation," Lab Chip, **15**(2), pp. 532–540.
[21] Lin, B. K., McFaul, S. M., Jin, C., Black, P. C., and Ma, H., 2013, "Highly Selective Biomechanical Separation of Cancer Cells From Leukocytes Using Microfluidic Ratchets and Hydrodynamic Concentrator," Biomicrofluidics, **7**(3), p. 034114.
[22] Hur, S. C., Henderson-MacLennan, N. K., McCabe, E. R. B., and Di Carlo, D., 2011, "Deformability-Based Cell Classification and Enrichment Using Inertial Microfluidics," Lab Chip, **11**(5), pp. 912–920.
[23] Yang, S., Lee, S. S., Ahn, S. W., Kang, K., Shim, W., Lee, G., Hyun, K., and Kim, J. M., 2012, "Deformability-Selective Particle Entrainment and Separation in a Rectangular Microchannel Using Medium Viscoelasticity," Soft Matter, **8**(18), pp. 5011–5019.
[24] Holmes, D., Whyte, G., Bailey, J., Vergara-Irigaray, N., Ekpenyong, A., Guck, J., and Duke, T., 2014, "Separation of Blood Cells With Differing Deformability Using Deterministic Lateral Displacement," Interface Focus, **4**(6), p. 20140011.
[25] Hvichia, G. E., Parveen, Z., Wagner, C., Janning, M., Quidde, J., Stein, A., Müller, V., Loges, S., Neves, R. P. L., Stoecklein, N. H., Wikman, H., Riethdorf, S., Pantel, K., and Gorges, T. M., 2016, "A Novel Microfluidic Platform for Size and Deformability Based Separation and the Subsequent Molecular Characterization of Viable Circulating Tumor Cells," Int. J. Cancer, **138**(12), pp. 2894–2904.
[26] Yeo, L. Y., and Friend, J. R., 2014, "Surface Acoustic Wave Microfluidics," Annu. Rev. Fluid Mech., **46**(1), pp. 379–406.
[27] Tian, Z., Yang, S., Huang, P.-H., Wang, Z., Zhang, P., Gu, Y., Bachman, H., Chen, C., Wu, M., Xie, Y., and Huang, T. J., 2019, "Wave Number–Spiral Acoustic Tweezers for Dynamic and Reconfigurable Manipulation of Particles and Cells," Sci. Adv., **5**(5), p. eaau6062.
[28] Zhang, S. P., Lata, J., Chen, C., Mai, J., Guo, F., Tian, Z., Ren, L., Mao, Z., Huang, P.-H., Li, P., Yang, S., and Huang, T. J., 2018, "Digital Acoustofluidics Enables Contactless and Programmable Liquid Handling," Nat. Commun., **9**(1), p. 2928.
[29] Li, P., and Huang, T. J., 2019, "Applications of Acoustofluidics in Bioanalytical Chemistry," Anal. Chem., **91**(1), pp. 757–767.
[30] Xie, Y., Bachman, H., and Huang, T. J., 2019, "Acoustofluidic Methods in Cell Analysis," TrAC Trends Anal. Chem., **117**, pp. 280–290.
[31] Wu, M., Ozcelik, A., Rufo, J., Wang, Z., Fang, R., and Jun Huang, T., 2019, "Acoustofluidic Separation of Cells and Particles," Microsystems Nanoeng., **5**(1), p. 32.
[32] Wu, M., Huang, P.-H., Zhang, R., Mao, Z., Chen, C., Kemeny, G., Li, P., Lee, A. V., Gyanchandani, R., Armstrong, A. J., Dao, M., Suresh, S., and Huang, T. J., 2018, "Circulating Tumor Cell Phenotyping Via High-Throughput Acoustic Separation," Small, **14**(32), p. 1801131.
[33] Ozcelik, A., Rufo, J., Guo, F., Gu, Y., Li, P., Lata, J., and Huang, T. J., 2018, "Acoustic Tweezers for the Life Sciences," Nat. Methods, **15**(12), pp. 1021–1028.
[34] Wu, M., Ouyang, Y., Wang, Z., Zhang, R., Huang, P.-H., Chen, C., Li, H., Li, P., Quinn, D., Dao, M., Suresh, S., Sadovsky, Y., and Huang, T. J., 2017, "Isolation of Exosomes From Whole Blood by Integrating Acoustics and Microfluidics," Proc. Natl. Acad. Sci., **114**(40), pp. 10584–10589.
[35] Augustsson, P., Magnusson, C., Nordin, M., Lilja, H., and Laurell, T., 2012, "Microfluidic, Label-Free Enrichment of Prostate Cancer Cells in Blood Based on Acoustophoresis," Anal. Chem., **84**(18), pp. 7954–7962.
[36] Antfolk, M., Magnusson, C., Augustsson, P., Lilja, H., and Laurell, T., 2015, "Acoustofluidic, Label-Free Separation and Simultaneous Concentration of Rare Tumor Cells From White Blood Cells," Anal. Chem., **87**(18), pp. 9322–9328.
[37] Franke, T., Braunmüller, S., Schmid, L., Wixforth, A., and Weitz, D. A., 2010, "Surface Acoustic Wave Actuated Cell Sorting (SAWACS)," Lab Chip, **10**(6), pp. 789–794.
[38] Bourquin, Y., Syed, A., Reboud, J., Ranford-Cartwright, L. C., Barrett, M. P., and Cooper, J. M., 2014, "Rare-Cell Enrichment by a Rapid, Label-Free, Ultrasonic Isopycnic Technique for Medical Diagnostics," Angew. Chem. Int. Ed., **53**(22), pp. 5587–5590.
[39] Collins, D. J., Alan, T., and Neild, A., 2014, "Particle Separation Using Virtual Deterministic Lateral Displacement (VDLD)," Lab Chip, **14**(9), pp. 1595–1603.
[40] Destgeer, G., Lee, K. H., Jung, J. H., Alazzam, A., and Sung, H. J., 2013, "Continuous Separation of Particles in a PDMS Microfluidic Channel Via Travelling Surface Acoustic Waves (TSAW)," Lab Chip, **13**(21), pp. 4210–4216.
[41] Ma, Z., Collins, D. J., and Ai, Y., 2016, "Detachable Acoustofluidic System for Particle Separation Via a Traveling Surface Acoustic Wave," Anal. Chem., **88**(10), pp. 5316–5323.
[42] Yunus, D. E., Sohrabi, S., He, R., Shi, W., and Liu, Y., 2017, "Acoustic Patterning for 3D Embedded Electrically Conductive Wire in Stereolithography," J. Micromech. Microeng., **27**(4), p. 045016.
[43] Shi, J., Ahmed, D., Mao, X., Lin, S.-C. S., Lawit, A., and Huang, T. J., 2009, "Acoustic Tweezers: Patterning Cells and Microparticles Using Standing Surface Acoustic Waves (SSAW)," Lab Chip, **9**(20), pp. 2890–2895.
[44] Ding, X., Peng, Z., Lin, S.-C. S., Geri, M., Li, S., Li, P., Chen, Y., Dao, M., Suresh, S., and Huang, T. J., 2014, "Cell Separation Using Tilted-Angle Standing Surface Acoustic Waves," Proc. Natl. Acad. Sci., **111**(36), pp. 12992–12997.
[45] Lei, J., Hill, M., de León Albarrán, C. P., and Glynne-Jones, P., 2018, "Effects of Micron Scale Surface Profiles on Acoustic Streaming," Microfluid. Nanofluid., **22**(12), p. 140.
[46] Lei, J., Glynne-Jones, P., and Hill, M., 2016, "Modal Rayleigh-Like Streaming in Layered Acoustofluidic Devices," Phys. Fluids, **28**(1), p. 012004.
[47] Bernassau, A. L., Chun-Kiat, Ong, Yong, Ma, Macpherson, P. G. A., Courtney, C. R. P., Riehle, M., Drinkwater, B. W., and Cumming, D. R. S., 2011, "Two-Dimensional Manipulation of Micro Particles by Acoustic Radiation Pressure in a Heptagon Cell," IEEE Trans. Ultrason. Ferroelectr. Freq. Control, **58**(10), pp. 2132–2138.
[48] Melde, K., Choi, E., Wu, Z., Palagi, S., Qiu, T., and Fischer, P., 2018, "Acoustic Fabrication Via the Assembly and Fusion of Particles," Adv. Mater., **30**(3), p. 1704507.
[49] Wu, M., Chen, K., Yang, S., Wang, Z., Huang, P. H., Mai, J., Li, Z., and Huang, T. J., 2018, "High-Throughput Cell Focusing and Separation via Acoustofluidic Tweezers," Lab Chip, **18**, pp. 3003–3010.
[50] Aghaamoo, M., Zhang, Z., Chen, X., and Xu, J., 2015, "Deformability-Based Circulating Tumor Cell Separation With Conical-Shaped Microfilters: Concept, Optimization, and Design Criteria," Biomicrofluidics, **9**(3), p. 034106.
[51] Bruus, H., 2012, "Acoustofluidics 2: Perturbation Theory and Ultrasound Resonance Modes," Lab Chip, **12**(1), pp. 20–28.
[52] Gorkov, L. P., 1962, "On the Forces Acting on a Small Particle in an Acoustical Field in an Ideal Fluid," Sov. Phys.-Dokl., **6**, pp. 773–775.
[53] Georgalis, Y., Philipp, M., Aleksandrova, R., and Krüger, J. K., 2012, "Light Scattering Studies on Ficoll PM70 Solutions Reveal Two Distinct Diffusive Modes," J. Colloid Interface Sci., **386**(1), pp. 141–147.
[54] Chen, B., Wang, B., Zhang, W. J., Zhou, G., Cao, Y., and Liu, W., 2013, "Macromolecular Crowding Effect on Cartilaginous Matrix Production: A Comparison of Two-Dimensional and Three-Dimensional Models," Tissue Eng., Part C, **19**(8), pp. 586–595.
[55] Rashid, R., Raghunath, M., and Wohland, T., 2011, "Macromolecular Crowding and Stem Cell Differentiation," Biophys. J., **100**(3), pp. 142a–143a.
[56] Zeiger, A. S., Loe, F. C., Li, R., Raghunath, M., and Van Vliet, K. J., 2012, "Macromolecular Crowding Directs Extracellular Matrix Organization and Mesenchymal Stem Cell Behavior," PLoS One, **7**(5), p. e37904.
[57] Pretlow, T. G., Boone, C. W., Shrager, R. I., and Weiss, G. H., 1969, "Rate Zonal Centrifugation in a Ficoll Gradient," Anal. Biochem., **29**(2), pp. 230–237.
[58] Boyum, A., 1964, "Separation of White Blood Cells," Nature, **204**(4960), pp. 793–794.
[59] Ulla, K., and Hallberg, T., 1983, "Separation of Lymphocyte Subsets by Expanding Velocity Sedimentation of E-Rosettes at Unit Gravity," J. Immunol. Methods, **59**, pp. 349–360.
[60] Wiklund, M., 2012, "Acoustofluidics 12: Biocompatibility and Cell Viability in Microfluidic Acoustic Resonators," Lab Chip, **12**(11), pp. 2018–2028.
[61] Ding, X., Lin, S.-C. S., Kiraly, B., Yue, H., Li, S., Chiang, I.-K., Shi, J., Benkovic, S. J., and Huang, T. J., 2012, "On-Chip Manipulation of Single Microparticles, Cells, and Organisms Using Surface Acoustic Waves," Proc. Natl. Acad. Sci., **109**(28), pp. 11105–11109.
[62] Kounis, N. G., Soufras, G. D., Tsigkas, G., and Hahalis, G., 2015, "White Blood Cell Counts, Leukocyte Ratios, and Eosinophils as Inflammatory Markers in Patients With Coronary Artery Disease," Clin. Appl. Thromb., **21**(2), pp. 139–143.
[63] Thavarajah, R., Mudimbaimannar, V., Rao, U., Ranganathan, K., and Elizabeth, J., 2012, "Chemical and Physical Basics of Routine Formaldehyde Fixation," J. Oral Maxillofac. Pathol., **16**(3), pp. 400–405.
[64] Kim, S.-O., Kim, J., Okajima, T., and Cho, N.-J., 2017, "Mechanical Properties of Paraformaldehyde-Treated Individual Cells Investigated by Atomic Force Microscopy and Scanning Ion Conductance Microscopy," Nano Converg., **4**(1), p. 5.